Electron acoustic waves in pure ion plasmas[a)]

F. Anderegg,[1,b)] C. F. Driscoll,[1] D. H. E. Dubin,[1] T. M. O'Neil,[1] and F. Valentini[1,2]
[1]*Department of Physics, University of California at San Diego, 9500 Gilman Drive, La Jolla, California 92093, USA*
[2]*Dipartimento di Fisica, Universita della Calabria, 87036 Arcavacata di Rende (CS), Italy*

(Received 4 December 2008; accepted 25 February 2009; published online 8 April 2009)

Standing electron acoustic waves (EAWs) are observed in a pure ion plasma. EAWs are slow nonlinear plasma waves; at small amplitude their phase velocities ($v_{ph} \simeq 1.4\bar{v}$ for small $k\lambda_D$) and their frequencies are in agreement with theory. At moderate amplitude, EAW-type plasma waves can be excited over a broad range of frequencies. This frequency variability comes from the plasma adjusting its velocity distribution so as to make the plasma mode resonant with the drive frequency. Wave-coherent laser-induced fluorescence shows the intimate nature of the wave-particle interaction, and how the particle distribution function is modified by the wave driver until the plasma mode is resonant with the driver. © *2009 American Institute of Physics*.
[DOI: 10.1063/1.3099646]

I. INTRODUCTION

Electron acoustic waves (EAWs) are the nonlinear low frequency branch of electrostatic plasma waves. The EAW typically has a phase velocity $v_{ph} \sim 1.4\bar{v}$ (for small $k\lambda_D$), quite low compared to typical plasma waves, and its frequency has a strong temperature dependence, $f_{EAW} \propto T^{1/2}$. Linear Landau damping would suggest that such slow phase velocity waves are strongly damped; but at finite wave amplitudes, trapping of particles near the phase velocity flattens the distribution function, resulting in a weakly damped wave. These wave have been studied theoretically[1,2] and numerically;[3] they have been observed in experiments with pure electron plasmas[4] and in laser-produced plasmas[5,6] and related numerical simulations.[7,8] In the case of the laser-produced plasma, the backscattered light indicates the presence of a fast wave, $v_{ph} \sim 4.2\bar{v}_e$, due to stimulated Raman scattering on Langmuir wave and a slow wave at $v_{ph} \sim 1.4\bar{v}_e$ identified as a stimulated EAW.

We observe that at small but finite amplitude, the EAW dispersion relation is correctly described by the approach of Holloway and Dorning.[1] In contrast at larger amplitude we observe that we can excite an EAW type wave at "any" frequency in the range of $1.4\bar{v} < v_{ph} < 2.1\bar{v}$; under these conditions, there is no simple dispersion relation for these waves. It is worth noting that this frequency variability seriously limits the temperature diagnostic capabilities of EAW since here f_{EAW} is not simply proportional to $T^{1/2}$.

Vlasov–Poisson simulations[9] have investigated the highly nonlinear amplitude regime, suggesting that EAW-like modes with strong harmonic content, called kinetic electrostatic electron nonlinear (KEEN) waves, can be excited over a wide range of frequencies.

With a chirped frequency drive[10] EAW-type plasma waves can also be excited over a continuous range of frequencies. These chirp driven waves were initially described as Bernstein–Green–Kruskal (BGK)-type plasma waves by Fajan's group at Berkeley. In this paper we show how the particle distribution $F(v)$ is strongly modified by a chirp drive.

II. EXPERIMENTAL APPARATUS

We study slow (EAW) and fast Trivelpiece–Gould (TG) waves in a pure ion plasma. We use a magnesium ion plasma confined in a Penning–Malmberg trap[11] with a uniform magnetic field $B=3$ T. Figure 1 shows the trap consisting of a series of hollow conducting cylinders of radius $R_w=2.86$ cm contained in ultrahigh vacuum at $P \approx 10^{-10}$ Torr. The ion density is $n \sim 1.5 \times 10^7$ cm^{-3}, over a radius $R_p \approx 0.45$ cm, with length $L_p \simeq 9$ cm. The plasma is held in steady state for days with a weak "rotating wall" electric field,[12] applied to the sectored electrode. The rotating wall is turned off about 100 ms before each wave measurement and is restored about 200 ms later.

A diagnostic laser beam parallel to the magnetic field close to the trap axis illuminates the plasma and laser-induced fluorescent (LIF) photons are collected by optics perpendicular to the trap axis. The diagnosed volume is the intersection of the laser beam with the viewing volume of the detection optics, corresponding to about a cylinder of length $\Delta z_L = 0.3$ cm and of radius $\Delta r_L \simeq 0.1$ cm. Individual detected photons emitted in the diagnosed volume are counted and their time of arrival recorded. The laser beam comes from a frequency-doubled dye laser and is tuned across the cyclic $^2S_{1/2}^{m_j=-1/2} \rightarrow {}^2P_{3/2}^{m_j=-3/2}$ (280 nm) transition from the ground state of singly ionized magnesium ions.

For the data presented here, the plasma has a laser measured Maxwellian velocity distribution with temperature controlled from $0.3 \text{ eV} < T < 1.5$ eV. These plasma parameters give the Debye length $0.1 \text{ cm} < \lambda_D < 0.24$ cm, thermal velocities $110 \text{ cm/ms} < \bar{v} < 245$ cm/ms, ion-ion collision rate $8 \text{ s}^{-1} > \nu_{ii} > 0.7 \text{ s}^{-1}$, and plasma frequency $f_p = 165$ kHz.

[a)]Paper UI1 3, Bull. Am. Phys. Soc. **53**, 281 (2008).
[b)]Invited speaker.

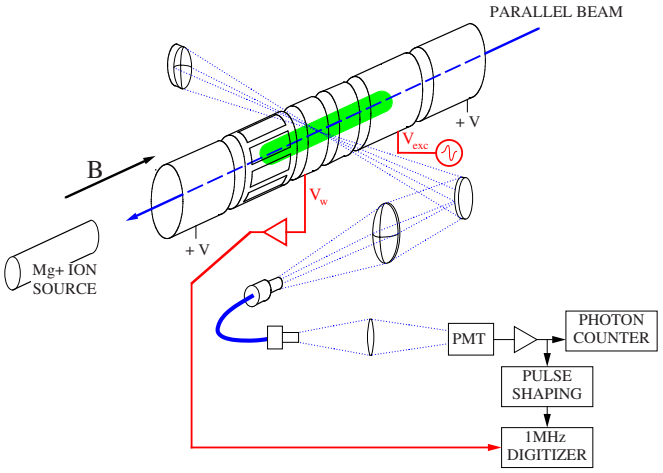

FIG. 1. (Color online) Experimental setup with coherent photon detection.

We excite standing EAW and TG waves with an electrode located near the end of the plasma column and detect the waves with a separate cylinder located near the other end of the plasma. Both excitation and detection electrodes are azimuthally symmetric and only excite and detect azimuthally symmetric modes ($m_\theta=0$). The modes presented in this paper have the longest possible axial wavelength ($m_z=1$), that is, $\lambda \approx 2L_p$ and the lowest radial mode number ($m_r=1$). The EAWs are excited by an amplitude-rounded burst $V_{\mathrm{exc}}(t)$ of ~ 100 cycles at a frequency f_{exc} and amplitude A_{exc}. Without amplitude rounding the TG wave is also excited by the harmonic content of the burst since the TG wave is substantially easier to excite and a few cycle burst is generally sufficient to excite a fast plasma mode.

The wave-induced wall voltage $V_w(t)$ is recorded and is fit in overlapping time segment as

$$V_w(t) = A_w(t)\cos[\theta_w(t)] \tag{1}$$

resulting in $\theta_w(t)$ with slowly varying $A_w(t)$ and frequency $f_w(t)=d\theta_w/2\pi dt$.

III. DISPERSION RELATION

In an infinite homogeneous unmagnetized plasma, the dispersion relation for an EAW of wavenumber $\mathbf{k}=k\hat{z}$ and frequency ω is

$$\omega_p^2 \mathcal{P}\int dv_z \frac{\partial F_0/\partial v_z}{v_z-\omega/k} = k^2, \tag{2}$$

where $\omega_p=\sqrt{4\pi e^2 n/m}$ is the plasma frequency.

$F_0(v_z)=\int dv_x dv_y F_0(\mathbf{v})$ is the equilibrium velocity distribution for velocity component v_z in the direction of $\mathbf{k}$ and

$$\mathcal{P}\int dv_z$$

stands for the principal part of the velocity integral.[1] If we replaced this integral with the Landau contour,[13] we would obtain the well-known dispersion relation for damped linear plasma waves. The principal part is used instead of the Landau contour because the waves have modified F_0, flattening the distribution over a small range of velocities around the phase speed ω/k. Assuming that F_0 is a Maxwellian distribution at temperature T, Eq. (2) may be solved for ω and the resulting "thumb diagram" is shown in Fig. 2(a). The upper branch is the traditional Langmuir wave starting at the plasma frequency for $k_z\lambda_D=0$. The lower branch (EAW) has an acoustic dispersion relation for small $k_z\lambda_D$.

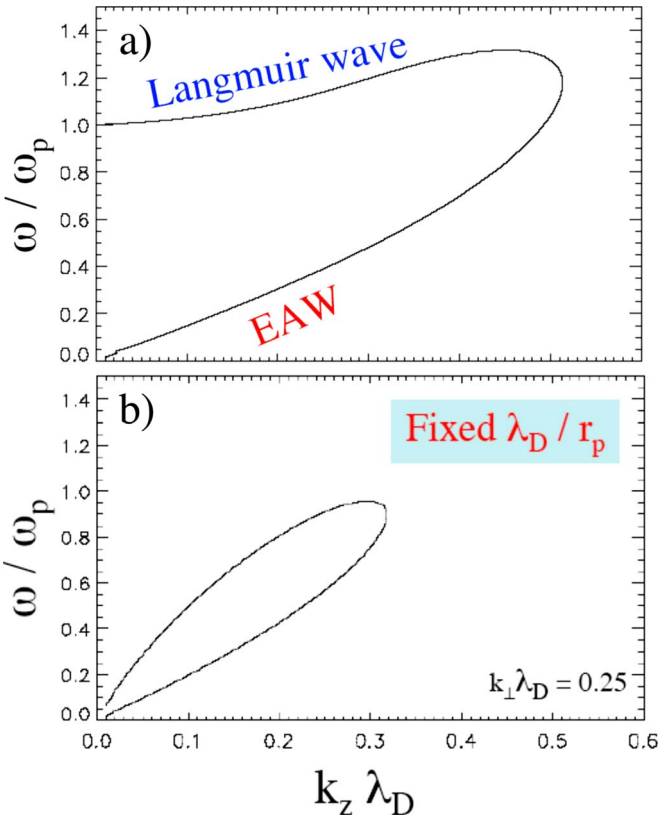

FIG. 2. (Color online) Plasma wave dispersion relation in: (a) homogeneous, infinite plasma; (b) plasma of finite radial size.

In a non-neutral plasma column confined in a Penning trap with uniform magnetic field $B\hat{z}$ and length L_p, the dispersion relation is modified. The waves become normal modes of the column at specific axial wavenumbers given approximately by $k_z=m_z\pi/L_p$, $m_z=0,1,2,\ldots$. The modes have an electrostatic potential structure of the form

$$\delta\phi(r,\theta,z) = \cos(k_z z)e^{im_\theta\theta}\Phi_{mk_z}(r), \tag{3}$$

where $\Phi_{m_\theta k_z}$ satisfies

$$\left[\frac{1}{r}\frac{\partial}{\partial r}r\frac{\partial}{\partial r} - \frac{m_\theta^2}{r^2} + \omega_p^2(r)\mathcal{P}\int \frac{dv_z\,\partial F_0/\partial v_z}{v_z-\omega/k_z}\right]\Phi_{m_\theta k_z}(r) = 0, \tag{4}$$

with boundary conditions that $\Phi \propto r^{m_\theta}$ near $r=0$ and $\Phi_{m_\theta k_z}=0$ at $r=R_w$, the radius of the surrounding grounded electrodes. Here $\omega_p(r)=\sqrt{4\pi e^2 n(r)/m}$ is the plasma frequency for density $n(r)$.

Equation (4) is an eigenvalue problem for the frequency ω and can be solved numerically for given F_0, m_θ, and k_z via the shooting method. For the case of a top-hat density profile with $n(r)=n_0$, when $r<R_p$ and zero otherwise, a solution to

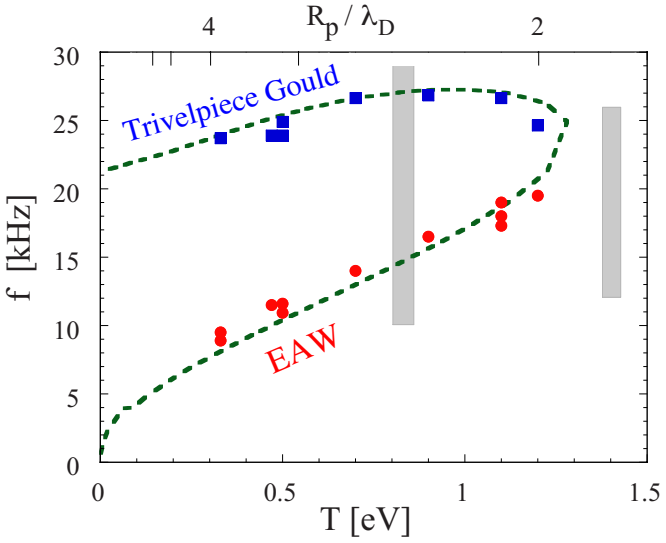

FIG. 3. (Color online) Plasma wave dispersion relation for finite radial size plasma and fixed k_z, plotted vs temperature.

Eq. (4) for $\Phi_{m_\theta k_z}(r)$ can be obtained in terms of Bessel functions. For $m_\theta=0$ and $k_z r_p \ll 1$, the solution reduces to

$$\Phi_{0k_z}(r)=\begin{cases} J_0[k_\perp(\omega,k_z)r], & r<R_p \\ J_0[k_\perp(\omega,k_z)R_p]\dfrac{\ln(R_w/r)}{\ln(R_w/R_p)}, & R_p<r<R_w, \end{cases} \tag{5}$$

where

$$k_\perp^2(\omega,k_z)=\omega_p^2 \mathcal{P}\int \frac{dv_z\,\partial F_0/\partial v_z}{v_z-\omega/k_z}-k_z^2. \tag{6}$$

The frequency ω must satisfy the condition that $\Phi'_{0k_z}(r)$ is continuous at $r=R_p$, which using Eq. (5) implies

$$k_\perp(\omega,k_z)J_1[k_\perp(\omega,k_z)R_p]=\frac{J_0[k_\perp(\omega,k_z)R_p]}{R_p\ln(R_w/R_p)}. \tag{7}$$

There are multiple solutions to Eq. (7) for ω, corresponding to normal modes with different numbers of radial nodes. For the mode with no radial nodes, the dispersion relation can be further simplified when $R_p/R_w \ll 1$. Then $k_\perp R_p \ll 1$ and the Bessel functions can be Taylor expanded, yielding

$$k_\perp(\omega,k_z)=\frac{1}{R_p}\left(\frac{2}{\ln(R_w/R_p)}\right)^{1/2}. \tag{8}$$

In Fig. 2(b) the solution of Eq. (8) for $\omega(k_z)$ [where Eq. (6) is used to determine $k_\perp(\omega,k_z)$] is plotted for the case where $k_\perp\lambda_D=0.25$ [i.e., $(\lambda_D/R_p)[2/\ln(R_w/R_p)]^{1/2}=0.25$]. The dispersion relation has a teardrop shape rather than a thumb shape because in a Penning trap both Langmuir waves and EAWs have acoustic-like dispersion relations at long wavelength.

In Fig. 3 this dispersion relation is plotted versus temperature at fixed $k_z=\pi/L_p$ (the lowest axial mode). Also, to compare the experiments it is important to use the actual radial density profile $n(r)$ rather than a top-hat profile, so in obtaining the dashed line of Fig. 3 the numerical shooting solution of Eq. (4) was employed.

When the amplitude is turned down sufficiently ($A_{\rm exc}\sim 50$ mV), the standing wave is observed at only one frequency, plotted in Fig. 3 as dots (EAW) and squares (TG wave) for different temperatures. The TG wave is easily excited with bursts as short as 3–10 cycles; in contrast the EAW requires typically hundreds of cycles to be excited. At small amplitude, these measurements are well described by the near-linear theory of Refs. 1 and 3. At temperatures above 1.3 eV, no waves are observed at comparably low excitation amplitude.

However, at larger amplitude the waves are excited over a range of frequencies; and furthermore, they ring at frequencies different than $f_{\rm EAW}$ or $f_{\rm exc}$ because the excitation has significantly modified the distribution function. The gray bar at $T=0.8$ eV shows the range of frequencies over which a 100 cycle burst with $A_{\rm exc}=300$ mV resulted in a wave $f_w=f_{\rm exc}$ ringing for hundreds of cycles. This means that at $T=0.8$ eV a wave can be excited at "any frequencies" within the vertical extent of the gray bar. This is not unexpected: theory has shown that any wavenumber is possible by choosing the appropriate trapped particle distribution.[13] Presumably physics of the experiment limits possible trapped particle distributions, therefore limiting the range of wave numbers. Buchanan *et al.*[14] and Holloway and Dorning[15] also noted that at finite amplitude many possible BGK states exist with a range of possible wavenumbers. Similarly, plasma waves at $T=1.4$ eV are excited with $A_{\rm exc}=200$ mV for 100 cycles, past the "end of the thumb" as shown by the gray bar where no near-linear solution exists. The drive modifies the particle distribution until the distribution becomes resonant with the drive. Naming waves in these continuous regimes is ill defined since wave names are generally given for well characterized distributions such as Maxwellian or near-Maxwellian distribution functions and beams. It is worth noting that Skiff *et al.*[16] observed a new branch of electrostatic wave on slightly non-Maxwellian plasmas.

Figure 4 shows the TG wave detected on a ring electrode resulting from a driving burst, consisting of 10 cycles at 21.5 kHz applied to the excitation electrode and the TG wave detected on a separate electrode. The received signal $V_w(t)$ grows smoothly during the burst.

Figure 5 shows excitation of an EAW wave, the driving burst applied to the excitation electrode, consisting of 100 cycles at 10.7 kHz, with ramped-up and ramped-down amplitude to avoid exciting a TG wave due to the harmonic contents of the burst. The signal received on the wall V_w is "erratic" during the exciting burst, reflecting the complicated process by which the particle distribution forms a plateau. If the driving burst is terminated after about 20 cycles, when A_w is the largest, the plasma oscillations damp within one or two wave cycles, presumably because the plateau was not formed yet. The EAWs are observed to damp exponentially

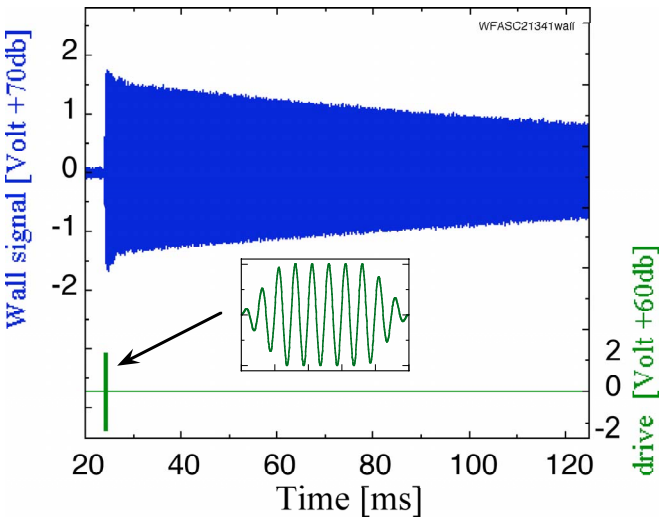

FIG. 4. (Color online) Detected TG wall signal $V_w(t)$ and drive burst $V_{exc}(t)$.

with $30<\gamma<3000$ s^{-1}; this is about ten times faster than TG waves of comparable amplitude.

Figure 6 illustrates how a $T\simeq 1$ eV plasma responds to a 100 cycle driving burst at a single frequency f_{exc} which is varied over the range $10<f_{exc}<30$ kHz, for four different excitation amplitudes. Figure 6(a) shows that with a 10 mV drive, only the TG wave is excited; with a 60 mV drive, Fig. 6(b) shows that the EAW and TG waves can be excited at their near-linear frequency. Figure 6(c) indicates that with a 100 mV drive, the plasma will sustain a wave over a range of driver frequencies around the EAW and the TG wave. Finally, Fig. 6(d) shows that with a driving burst of 300 mV the plasma can sustain a wave at any frequency within the range of 10–30 kHz.

The arrows under Fig. 6(b) show the nonlinear shift in frequency, from the excitation frequency f_{exc} (bottom) to the plasma response frequency f_{res} (top). A linear harmonic oscillator only rings at its natural frequency, whereas the plasma response shows clear, reproducible frequency shifts. In the vicinity of the TG mode, the plasma responds with a frequency closer to the TG mode than the drive. In contrast,

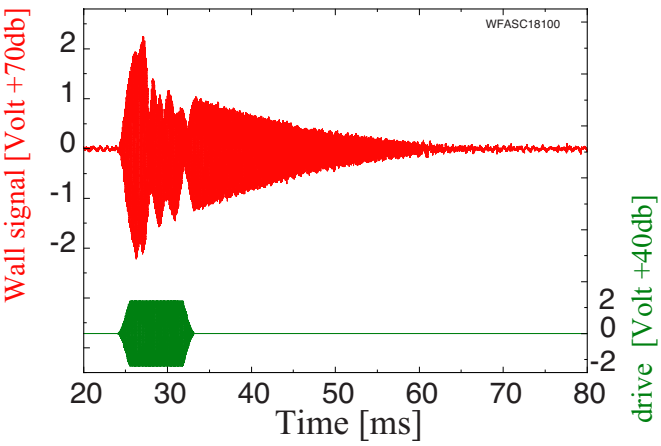

FIG. 5. (Color online) Detected EAW wall signal $V_w(t)$ and 100 cycles drive burst $V_{exc}(t)$.

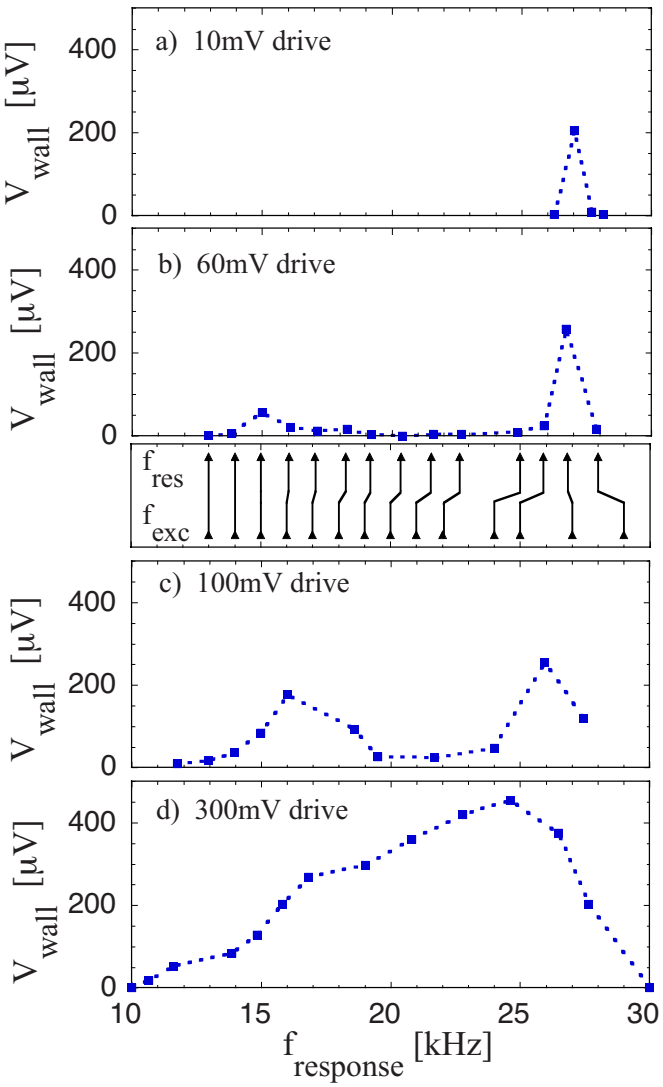

FIG. 6. (Color online) Received signal size vs received frequency for four different drive amplitudes.

around the EAW frequency the plasma responds at the driver frequency; that is, the particle distribution rearranges itself until the mode is resonant with the drive.

Figure 7 shows the LIF-measured ion distribution function. When the driver frequency matches the TG resonant frequency (21.8 kHz) for a Maxwellian particle distribution, the distribution remains essentially unchanged by the wave [Fig. 7(a)]. In contrast, when the driver is below the TG resonant frequency, Fig. 7(b) shows the distribution function rearranged so as to make the drive resonant. The arrow indicates the phase velocity of the excited standing wave. The solid line is a Maxwellian fit to the measured distribution before the wave. The data suggest that when the driver frequency does not match the resonant frequency of a Maxwellian distribution, some of the driver energy is transferred to the particles to rearrange them in a new distribution. In contrast, a resonant driver appears to couple to the wave electric field and the oscillatory motion of the particles at the wave driver frequency.

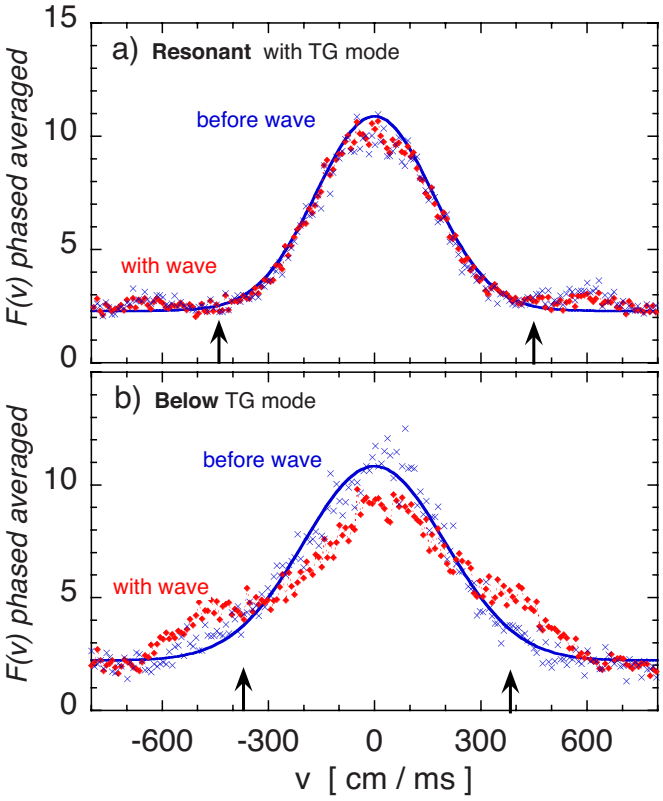

FIG. 7. (Color online) (a) TG mode driven on resonance at $f_{\text{drive}}=21.8$ kHz; (b) TG mode driven below resonance at $f_{\text{drive}}=19$ kHz.

IV. STANDING WAVE MODEL

We model standing waves in the trap as two superimposed independent waves of amplitude ϕ_1 with opposite v_{ph}, each perturbing and trapping particles in *separate* Maxwellian distributions. The steady-state model distribution conserves energy $\varepsilon=\frac{1}{2}mv^2+q\phi(z)$ separately in each wave frame defined by $w=v\pm v_{\text{ph}}$. A smooth transition from trapped ($\varepsilon<q\phi_1$) to untrapped ($\varepsilon>q\phi_1$) particles is modeled by[17]

$$F_{\pm}\equiv\begin{cases}\exp\left\{-\left(q\phi_1+\frac{1}{2}mv_{\text{ph}}^2\right)/T\right\}, & \text{for } \varepsilon<q\phi_1\\ \exp\left\{-\left(-\varepsilon+\frac{1}{2}mv_{\text{ph}}^2\mp v_{\text{ph}}u(\varepsilon)\right)/T\right\}, & \text{for } \varepsilon>q\phi_1,\end{cases} \tag{9}$$

where $\pm$ represent positive and negative v_{ph}, $u(\varepsilon)\equiv\int_{q\phi_1}^{\varepsilon}d\varepsilon'/I(\varepsilon')$, and $I(\varepsilon)\equiv\int_0^L(dz/L_p)[2\varepsilon-2q\phi(z)]^{1/2}$. The complete particle distribution is

$$F=F_+ + F_- - F_0, \tag{10}$$

where F_0 is the unperturbed Maxwellian, and F_+ and F_- each consists of an unperturbed Maxwellian and a wave contribution.

For a single traveling wave, linear theory predicts that the parallel wave electric field E_z creates a perturbation to $F(v)$ as

$$F_{\pm}(v,z,t)=F_0+\frac{\partial F_0/\partial v}{v-v_{\text{ph}}}\frac{qE_z}{mk_z}\cos(k_z z\mp\omega t). \tag{11}$$

Clearly the perturbation due to particles faster than v_{ph} has a different sign than for particles slower than v_{ph}. This partial cancellation leads to a reduction of the velocity-integrated perturbation δn. The term $\partial F_0/\partial v$ also leads to a sign change at $v=0$.

Finally, the model is smoothed to the spatial and velocity definition of the experiment with $\delta z/L_p\sim 1/20$ and $\delta v/2\bar{v}\sim 1/20$. Although simplistic in some details, this model contains the essence of particle trapping and two-wave superposition required to interpret the measurements. For example, the discontinuity at v_{ph} of Eq. (11) is mitigated by the trapping width Δv_T setting a lower limit for $v-v_{\text{ph}}$, by the presence of two waves, and by the experimental resolution.

V. COHERENT PARTICLE DISTRIBUTION MEASUREMENT

The LIF data allow us to construct the particle distribution function $F(v,\theta)$ coherent with the wave phase $\theta_w(t)$ received on the wall. The excitation laser propagates axially at $r=0$, with frequency tuned to be resonant with particles of velocity v_ℓ. The individual fluorescent photons emitted from the central axial region (-0.15 cm$<z<0.15$ cm) of the plasma are detected. The rate of detected photons is $P(v_\ell,t)$ representing $F(v_\ell,z=0,t)$ and the correlation integral

$$\delta F^{\text{coh}}(v_\ell)=\int_{t_1}^{t_2}dt\left(\frac{P(v_\ell,t)}{t_2-t_1}\right)\cos[\theta_w(t)-\theta_{w0}] \tag{12}$$

is calculated for period t_2-t_1 encompassing about 1000 photons over about 100 wave cycles. Repeating this process for 250 velocities v_ℓ results in $\delta F^{\text{coh}}(v_\ell)$. Each measurement is on the same plasma, after waiting 3–10 s for the plasma to re-equilibrate.

Figure 8(a) shows the wave-phase coherent $\delta F^{\text{coh}}(v)$ in the presence of a moderate amplitude standing EAW at 10.7 kHz; here in units of coherent photons per millisecond for 1 mW of laser illumination. The change of sign at $v=0$ comes from the $\partial F/\partial v$ term, and the sign change at $\pm v_{\text{ph}}$ comes from the $(v-v_{\text{ph}})$ term in the denominator of Eq. (11). The zero crossings at $\pm v_{\text{ph}}$ are an experimental measurement of the standing wave-phase velocity. Here $v_{\text{ph}}=\pm 208$ cm/ms gives $\frac{1}{2}\lambda=v_{\text{ph}}/2f=9.7$ cm; this is about 10% longer than L_p, as is typical of standing plasma waves in traps.[18] The solid line is the result of the model of Sec. IV.

Figure 8(b) shows the particle distribution $F_0(v)$ before the wave, with a temperature $T=0.31$ eV. As the wave damps, the wave energy is transferred to the particles resulting in a temperature increase to $T=0.44$ eV 100 ms later. A similar wave-coherent LIF technique gives the distribution at various wave phases, $F(v,\theta_j)$. This is obtained by binning the received photons into eight wave-phase bins $\theta_j=2\pi j/8$.

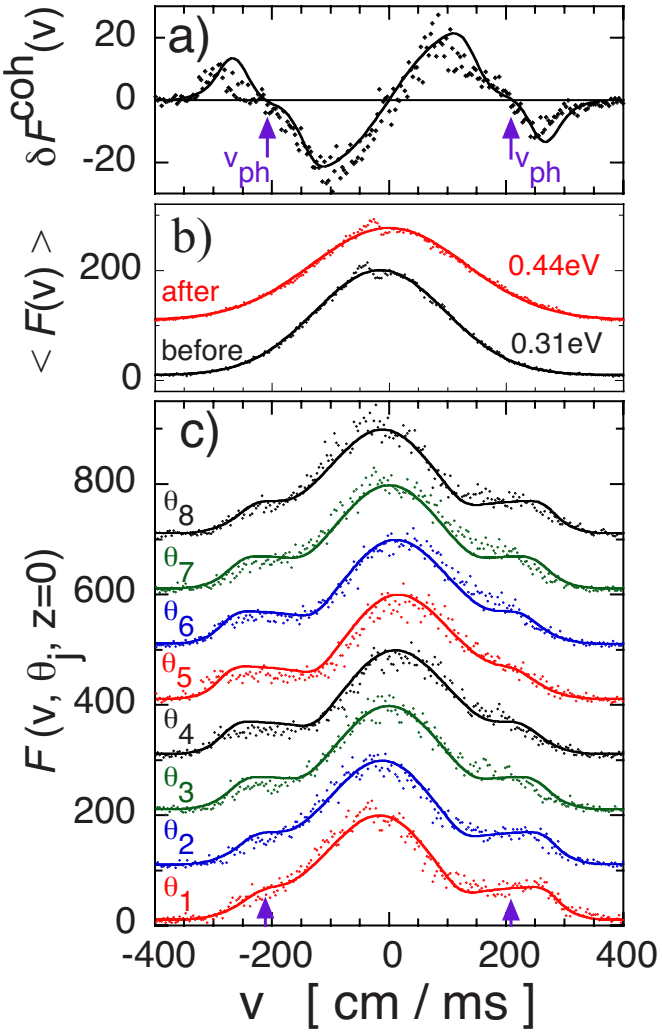

FIG. 8. (Color online) (a) Coherent particle response $\delta F(v)$. (b) Phase average particle distribution before and after EAW. (c) Phase-coherent particle distribution in the presence of an EAW with $v_{ph}=208$ cm/ms.

Here also the measurement is done at $r\simeq 0$, $z=0$. Figure 8(c) shows the particle distribution $F(v,\theta_j)$ for eight phases of the wave. To obtain these we accumulate photons in their respective phase bin for 10 ms, that is ~100 wave cycles. $F(v,\theta_j)$ show two plateaus, corresponding to the particles trapped by the wave at $\pm v_{ph}$. The widest plateaus Δv_T are observed at phase $\theta_j=1$ and 5. These wave-trapped particles propagate in the wave troughs past the photon detector at $z=0$, and reflect at the plasma ends, remaining trapped during hundreds of end reflections. Figure 8(c) also shows clearly the oscillations back and forth (δv_0) of low velocity (non-trapped) particles. Note that for TG waves the entire distribution is oscillating since the phase velocity is located outside of the particle distribution.

The solid curves in Fig. 8(c) are the result of the standing wave model. This particle distribution can be represented as a contour plot of $F(v,\theta,z=0)$, as shown in Fig. 9. This plot resembles a phase space plot, $F(v,z;t=0)$, but all the measurements of this standing wave are made at $z=0$. Figure 9 clearly shows the particle trapping over an extent Δv_T in 2 waves with $\pm v_{ph}=\pm 208$ cm/ms. The oscillations of particles around $v=0$ are also clearly visible and labeled δv_0. Δv_T and δv_0 both result from the wave electric field, and are related by $\Delta v_T^2=2\delta v_0 v_{ph}$.

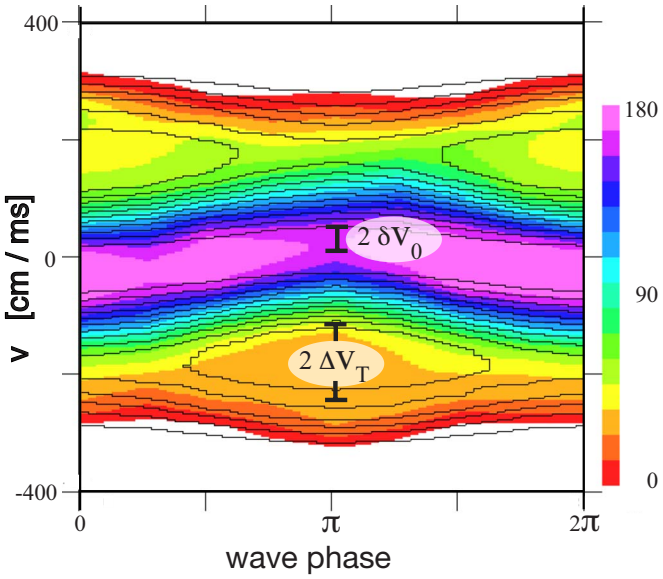

FIG. 9. (Color online) Contour plot of $F(v,\theta_j)$ measured at $z=0$.

VI. CHIRPED DRIVE, EXTREME MODIFICATION OF $F(v)$

Similar plasma modes can also be excited to very large amplitude by a downchirped frequency drive.[10] Here the chirped frequency creates extreme modification of $F(v)$, and can be tailored to support a mode at almost any frequency. Figure 10 shows an example of extreme modification of $F(v)$ from an amplitude-rounded ($A_{exc}\approx 800$ mV) burst of 14.5 cycles total, chirped from 20 to 9 kHz. Here, the original Maxwellian distribution has been essentially split into two counterpropagating distributions, each supporting an EAW-like wave on the "inside" of $F(v)$. This wave rings at $f_w=9.9$ kHz, with an amplitude giving $\delta n/n\sim 0.3$, with very weak damping $\gamma\approx 0.5$ s^{-1}, $\gamma/\omega\sim 10^{-5}$.

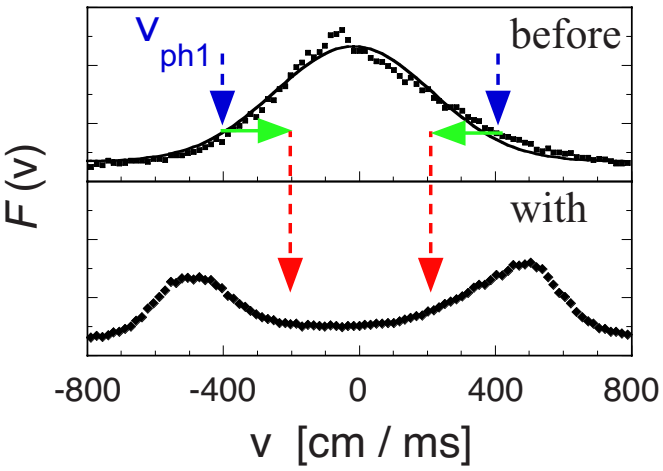

FIG. 10. (Color online) $F(v)$ before chirped down driven wave and with the plasma wave.

This double hump particle distribution is stable according to Penrose criteria.[13] Penrose criteria predicts that the plasma is unstable if $\int_{-\infty}^{+\infty}[[F(v_0)-F(v)]/(v-v_0)^2]dv<0$ and k satisfies $k^2<\omega_p^2\int_{-\infty}^{+\infty}[[F(v_0)-F(v)]/(v-v_0)^2]dv$. The first condition is satisfied by the resulting double hump distribution but our k is dominated by $k_\perp$ and is larger by a factor 2 than the maximum allowed by Penrose criteria. Similar frequency sweeping of phase space structures has been studied theoretically and numerically,[2,19] and driven phase space "holes" have been numerically explored[19] as an explanation for observations of almost-undamped plasma waves in trapped systems.[20]

VII. DISCUSSION

We have observed near-linear plasma waves with a phase velocity slow enough to be located in the bulk of the particle velocity distribution, generically called EAWs. At small amplitude, the experimentally observed standing wave frequencies confirm the theory concept of Holloway and Dorning presuming a local flattening of the particle distribution around the phase velocity. At moderate and large amplitude, the waves can be excited over a wide continuum range of frequencies. Here the wave driver modifies the particle velocity distribution until the distribution becomes resonant with the drive. The observed mode frequency is still surprisingly well described by the Dorning theoretical approach using the modified particle distribution, even for the large amplitude case. For example, using one of the measured velocity distributions of Fig. 8, Dorning theory predicts $v_{ph}/\bar{v}=1.85$ compared to the coherently measured $v_{ph}/\bar{v}=1.86$.

ACKNOWLEDGMENTS

We thank Dr. B. Afeyan and Dr. R. W. Gould for stimulating discussions.

This work was supported by the National Science Foundation under Grant No. PHY-0354979 and the NSF/DOE under Grant No. PHY-0613740.

[1] J. P. Holloway and J. J. Dorning, Phys. Rev. A **44**, 3856 (1991).
[2] H. Schamel, Phys. Plasmas **7**, 4831 (2000).
[3] F. Valentini, T. M. O'Neil, and D. H. E. Dubin, Phys. Plasmas **13**, 052303 (2006).
[4] A. A. Kabantsev, F. Valentini, and C. F. Driscoll, AIP Conf. Proc. **862**, 13 (2006); F. Valentini, T. M. O'Neil, and D. H. E. Dubin, *ibid.* **862**, 3 (2006).
[5] D. S. Montgomery, R. J. Focia, H. A. Rose, D. A. Russell, J. A. Cobble, J. C. Fernndez, and R. P. Johnson, Phys. Rev. Lett. **87**, 155001 (2001).
[6] N. J. Sircombe, T. D. Arber, and R. O. Dendy, Plasma Phys. Controlled Fusion **48**, 1141 (2006).
[7] Lj. Nikolić, M. M. Škorić, S. Ishiguro, and T. Sato, Phys. Rev. E **66**, 036404 (2002).
[8] A. Ghizzo, T. W. Johnston, T. Révéille, P. Bertrand, and M. Albrecht-Marc, Phys. Rev. E **74**, 046407 (2006).
[9] B. Afeyan, K. Won, V. Savchenko, T. W. Johnston, A. Ghizzon, and P. Bertrand, in *Proceedings of the Inertial Fusion Sciences and Applications 2003*, edited by B. A. Hamel, D. D. Meyerhofer, J. Meyer-ter-Vehn, and H. Azechi (American Nuclear Society, Monterey, 2004), p. 213.
[10] W. Bertsche, J. Fajans, and L. Friedland, Phys. Rev. Lett. **91**, 265003 (2003); F. Peinetti, W. Bertsche, J. Fajans, J. Wurtele, and L. Friedland, Phys. Plasmas **12**, 062112 (2005).
[11] F. Anderegg, X.-P. Huang, E. Sarid, and C. F. Driscoll, Rev. Sci. Instrum. **68**, 2367 (1997).
[12] X.-P. Huang, F. Anderegg, E. M. Hollmann, C. F. Driscoll, and T. M. O'Neil, Phys. Rev. Lett. **78**, 875 (1997); F. Anderegg, E. M. Hollmann, and C. F. Driscoll, *ibid.* **81**, 4875 (1998); E. M. Hollmann, F. Anderegg, and C. F. Driscoll, Phys. Plasmas **7**, 2776 (2000).
[13] N. A. Krall and A. W. Trivelpiece, *Principles of Plasma Physics* (McGraw-Hill, New York, 1973).
[14] M. L. Buchanan, J. P. Holloway and J.J. Dorning, *Nonlinear and Relativistic Effects in Plasmas: Papers Presented at the Topical Conference on Research Trends in Nonlinear and Relativistic Effects in Plasmas*, San Diego, 5–8 February 1990, Research Trends in Physics, edited by V. Stefan (American Institute of Physics, New York, 1992), Vol. I, p. 601.
[15] J. P. Holloway and J. J. Dorning, *Modern Mathematical Methods in Transport Theory (Operator Theory): Advances and Applications*, edited by W. Greenberg and J. Polewczak (Birkhäuser Verlag, Basel, 1991), Vol. 51, p. 155.
[16] F. Skiff, H. Gunell, A. Bhattcharjee, C. S. Ng, and W. A. Noonan, Phys. Plasmas **9**, 1931 (2002).
[17] V. E. Zakharov and V. I. Karpman, Sov. Phys. JETP **16**, 351 (1963).
[18] J. K. Jennings, R. L. Spencer, and K. C. Hansen, Phys. Plasmas **2**, 2630 (1995).
[19] D. Y. Eremin and H. L. Berk, Phys. Plasmas **9**, 772 (2002); H. L. Berk, B. N. Breizman, and N. V. Petviashvilli, Phys. Lett. A **234**, 213 (1997).
[20] L. Friedland, F. Peinetti, W. Bertsche, J. Fajans, and J. Wurtele, Phys. Plasmas **11**, 4305 (2004); I. Barth, L. Friedland, and A. G. Shagalov, *ibid.* **15**, 082110 (2008).